

# ADAPTIVE SPECTRAL VISCOSITY FOR HYPERBOLIC CONSERVATION LAWS

EITAN TADMOR AND KNUT WAAGAN

ABSTRACT. Spectral approximations to nonlinear hyperbolic conservation laws require dissipative regularization for stability. The dissipative mechanism must on the other hand be small enough, in order to retain the spectral accuracy in regions where the solution is smooth. We introduce a new form of viscous regularization which is activated only in the local neighborhood of shock discontinuities. The basic idea is to employ a spectral edge detection algorithm as a dynamical indicator of where in physical space to apply numerical viscosity. The resulting spatially local viscosity is successfully combined with spectral viscosity, where a much higher than usual cut-off frequency can be used. Numerical results show that the new Adaptive Spectral Viscosity scheme significantly improves the accuracy of the standard spectral viscosity scheme. In particular, results are improved near the shocks and at low resolutions. Examples include numerical simulations of Burgers' equation, shallow water with bottom topography and the isothermal Euler equations. We also test the schemes on a non-convex scalar problem, finding that the new scheme approximates the entropy solution more reliably than the standard spectral viscosity scheme.

## 1. INTRODUCTION - MAIN INGREDIENTS

Let  $u(\cdot) : (-\pi, \pi) \mapsto \mathbb{R}$  be a  $2\pi$ -periodic function and let  $u_N \equiv P_N u(x)$  denote its pseudospectral approximation of order  $N$ ,

$$(1.1a) \quad u_N(x) = P_N u(x) := \sum_{k=-N}^N \widehat{u}_k e^{ikx}, \quad \widehat{u}_k = \sum_{j=-N}^N u(x_j) e^{-ikx_j} \frac{\Delta x}{2\pi},$$

which is based on the equidistant sample points

$$(1.1b) \quad x_j = \left(j - \frac{1}{2}\right) \Delta x, \quad \Delta x = \frac{2\pi}{2N + 1}.$$

If  $u \in C^\infty$ , the Fourier approximation enjoys infinite (i.e. spectral) order of accuracy. When applied to functions that are only piecewise smooth, however, this property breaks down even in the smooth regions. Around a discontinuity,  $\mathcal{O}(1)$  Gibbs' oscillations are observed, and only first order convergence  $\mathcal{O}(1/N)$  is obtained in the smooth regions. The spectral order of accuracy can be recovered by filtering techniques which we will refer to as post-processing [1, 6, 18]. Since the filtering requires explicit knowledge of the locations of singularities, algorithms for detecting edges from spectral data have been developed [2, 18].

We consider conservation laws

$$(1.2) \quad u_t + f(u)_x = 0, \quad u(\cdot, t) : (-\pi, \pi) \mapsto \mathbb{R},$$

subject to  $2\pi$ -periodic initial data  $u_0(x)$ . A straightforward pseudospectral approximation of (1.2) takes the form

$$(1.3) \quad (u_N)_t + (P_N f(u_N))_x = 0.$$

Since solutions of (1.2) develop shock discontinuities at a finite time, Gibbs' phenomena will render the pseudospectral method (1.3) inaccurate or even unstable [16]. The instability can be addressed by the classical vanishing viscosity method, which is given by

$$(1.4) \quad (u_N)_t + (P_N f(u_N))_x = \epsilon_N (u_N)_{xx}, \quad \epsilon_N = \mathcal{O}(1/N).$$

*Date:* June 3, 2011.

*1991 Mathematics Subject Classification.* 35L60, 35L67, 65M70.

*Key words and phrases.* Nonlinear Conservation Laws, Spectral Viscosity, Edge Detection.

Research was supported by grants from the Office of Naval Research ONR#N000140910385, and the National Science Foundation DMS#10-08397.

It yields a stable the scheme, but obviously involves a first order error  $\mathcal{O}(1/N)$ . Thus, stability is gained at the expense of sacrificing spectral accuracy.

**1.1. Spectral viscosity.** In order to retain both high accuracy and stability, the spectral viscosity (SV) method was introduced in [16],

$$(1.5) \quad (u_N)_t + (P_N f(u_N))_x = \epsilon_N Q * (u_N)_{xx}, \quad Q(x) := \sum_{|k| \leq N} \widehat{Q}_k e^{ikx}.$$

The coefficient  $\epsilon_N$  represents the magnitude of diffusion, and will be set to  $\epsilon_N = \mathcal{O}(1/N)$ . The viscosity kernel  $Q$  is chosen so as to filter out the large scales from the diffusion operator. Spectral accuracy is ensured by leaving enough large scale modes without dissipation, i.e.  $\widehat{Q}_k = 0$  for  $|k| < m$  with the cutoff frequency  $m$  increasing appropriately with  $N$ . We use

$$(1.6) \quad Q(x) = \sum_{|k| > m} \exp\left(-\left(\frac{N-k}{k-m}\right)^2\right) e^{ikx},$$

and unless otherwise noted, we let  $m = \sqrt{N}$ , which results in a stable scheme (e.g. [11, 12, 16, 14, 15]). The resulting SV method reads

$$(1.7) \quad \text{SV} \quad \mapsto \quad (u_N)_t + (P_N f(u_N))_x = -N \sum_{|k| > m} \frac{k^2}{N^2} \widehat{Q}_k \widehat{u}_k(t) e^{ikx}, \quad \widehat{Q}_k = \exp\left(-\left(\frac{N-k}{k-m}\right)^2\right).$$

The parameterization  $m \sim \sqrt{N}$  corresponds to the second-order diffusion in the vanishing viscosity regularization in (1.4). A more general setup, based on *hyper-viscosity* of order  $2s$  was introduced in [17],

$$(1.8) \quad \text{HyperSV} \quad \mapsto \quad (u_N)_t + (P_N f(u_N))_x = -N \sum_{|k| > m} \eta \left(\frac{|k|}{N}\right) \widehat{u}_k(t) e^{ikx}, \quad \eta(\xi) \geq \max\left\{\xi^{2s} - \frac{c}{N}, 0\right\}.$$

The case  $s = 1$  corresponds to the usual SV method. As  $s$  increases, the resulting HyperSV is activated at smaller portions of the spectrum,  $|k| > m \sim N^{(2s-1)/(2s)}$  and its stability was proved in [17]. In particular, this allows us to parametrize the cut-off  $m$  as a fixed fraction of  $N$ , which will be advocated below. In closing, we note that the SV and HyperSV methods have been generalized to non-periodic problems in [10, 7, 9].

**1.2. Post-processing.** As pointed out in [10, 13], the SV solution  $u_N$  is better viewed as an approximation to the Fourier projection  $P_N u(\cdot, t)$ , rather than to the exact solution  $u(\cdot, t)$  itself. The total error

$$(1.9) \quad u_N - u \equiv (u_N - P_N u) + (P_N u - u),$$

will therefore be dominated by the interpolation error  $P_N u - u$  which is  $\mathcal{O}(1/N)$  due to Gibbs oscillations. Nevertheless, spectral accuracy of  $P_N u$  can be recovered by postprocessing in smooth regions. Hence, we expect that spectral accuracy of the SV solution  $u_N$  can be recovered in the same way. Following [19, 21], a post-processed SV solution, denoted  $\tilde{u}_N$ , will be recovered from  $u_N$  by a convolution with a proper mollifier,  $M(\xi)$ ,

$$(1.10a) \quad \tilde{u}_N(x) = \int_{-\infty}^{\infty} \frac{1}{\theta} M\left(\frac{x-y}{\theta}\right) u_N(y) dy \quad M(\xi) := \rho(\xi) D_p(\xi).$$

Here,  $D_p$  is the usual Dirichlet kernel of degree  $p$

$$(1.10b) \quad D_p(\xi) = \frac{\sin[(p + \frac{1}{2})\xi]}{\sin[\frac{1}{2}\xi]},$$

and  $\rho$  is the smooth weighting function locally supported in  $[-\pi, \pi]$

$$(1.10c) \quad \rho(\xi) = \bar{\rho} \exp\left(-\frac{10\xi^2}{(\pi^2 - \xi^2)_+}\right)$$

with the normalization factor  $\bar{\rho}$  chosen so that  $\rho$  has unit mass,

$$(1.10d) \quad \int_{-\infty}^{\infty} M(\xi) d\xi = 1.$$

There are two parameters to be chosen:

1. The degree  $p$  in (1.10b) is set to be a fraction of  $N$ ; we use  $p = 0.5586\theta N$  as suggested in [21].

2. The scaling factor  $\theta$  dictates the active neighborhood of mollification,  $[x - \theta\pi, x + \theta\pi]$  in (1.10). Note that  $\theta$  can depend on  $x$ . Indeed, we will take  $\theta(x) = \text{dist}(x, \mathcal{S}(u))/\pi$ , where  $\mathcal{S}(u)$  is the set of singular points of  $u$ . In the next section we describe an algorithm to find  $\mathcal{S}(u)$  from  $u_N$ .

**1.3. Spectral edge detection.** As seen in the previous section, postprocessing requires explicit knowledge of the spatial location of discontinuities. One needs to know the interval of smoothness surrounding each point  $x$  so that  $\theta(x)$  in (1.10) can be computed. To this end, the locations, as well as the magnitudes, of discontinuities may be extracted from spectral data by using the following edge detection algorithm from [2, 3, 18]. Let  $K(u_N)$  be the concentration kernel

$$(1.11a) \quad K(u_N)(x) = \sum_{|k| \leq N} \text{sign}(k) \sigma_k \hat{u}_k e^{ikx},$$

where the so called concentration factors,  $\sigma_k \equiv \sigma(|k|/N)$ , are normalized such that

$$(1.11b) \quad \sum_{k=1}^N \frac{\sigma(k/N)}{k} = 1.$$

The idea behind the concentration kernel is to provide a function  $K(u_N)$  that vanishes in smooth regions of  $u$ , and equals the (signed) magnitude of the jump discontinuity at the jump location. Here, we take the concentration kernel

$$(1.11c) \quad \sigma(\xi) = \bar{\sigma}(1 - \cos \pi\xi),$$

where (1.11b) determines the normalization factor

$$(1.11d) \quad \bar{\sigma} = \left( \sum_{k=1}^N \frac{1 - \cos \frac{\pi k}{N}}{k} \right)^{-1}.$$

This choice of  $\sigma$  yields an accurate localizer  $K(u_N)$  that has some oscillations near the discontinuities.

In order to pinpoint the shock locations, the authors of [3] suggested a resolution-dependent lower threshold for which  $K(u_N)$ -values that signify a shock. They consider the enhanced spectral concentration kernel given by

$$(1.12a) \quad K_\delta(u_N)(x) = \chi_\delta[K(u_N)],$$

where

$$(1.12b) \quad \chi_\delta[\xi] := \begin{cases} 0, & |\xi| \leq \delta, \\ \xi, & |\xi| > \delta, \end{cases}$$

is a cut-off function parameterized by the cut-off magnitude  $\delta$ . The cut-off  $\delta$  will typically depend on  $N$ . The underlying assumption is that there is a scale separation between the shock magnitude and the local variation in the smooth data, and these scales should be reflected in the cut-off  $\delta$ . This cut-off technique was used in [4] to provide shock locations for post-processing, i.e. to specify  $\theta$  in (1.10). In the next section we will introduce a new application of this shock detection method: We will use it as a *dynamical* indicator of where in physical space to activate spectral diffusion.

## 2. NEW ALGORITHMS - FROM EDGE DETECTION TO ADAPTIVE VISCOSITY

Our basic intuition is that we want to avoid numerical diffusion in the smooth regions, while we want to ensure that there is enough of it in the local neighborhood of shocks. To accomplish this we employ the localizer  $K(u_N)$  as a local diffusion coefficient, letting

$$(2.1) \quad (u_N)_t + (P_N f(u_N))_x = \epsilon_N |K(u_N)| \cdot (u_N)_{xx}.$$

Note however, that  $K(u_N)$  need not be spectrally small in the smooth region, hence (2.1) does not lead to a spectrally accurate scheme. In order to retain spectral accuracy in smooth regions we cut off the localizer  $K_N$  below a small threshold in the spirit of the enhanced edge detector (1.12). Other factors may also make  $K(u_N)$  unsuitable, for example it will be oscillatory near the discontinuities.

Thus, in order to obtain a more suitable local diffusion coefficient we consider a modified localizer  $L(u_N)$ . The modification can be broken down into the following steps:

- i) First evaluate  $|K(u_N)|$  to ensure a positive viscosity amplitude, as already indicated in (2.1).

- ii) Next, we truncate to enforce  $|K(u_N)| \leq 1$ , since we want to control the largest possible magnitude of the diffusion coefficient. Neglecting this may produce restrictions on the step size when discretizing in time.
- iii) We then mollify the result with a small width  $\lambda = \mathcal{O}(1/N)$ . This eliminates small scale oscillations in  $K(u_N)$ .
- iv) We renormalize so that the maximum of  $\min(1, K(u_N))$  before mollification is retained, since that is the true measure of shock strength.
- v) Any value smaller than  $\delta = \mathcal{O}(1/N)$  is set to 0. This cut-off is crucial, since  $K(u_N)$  need not be spectrally small away from the discontinuities<sup>1</sup>.

The resulting modified localizer  $L_N$  reads

$$(2.2a) \quad L(u_N) \equiv \chi_\delta [C\mu_\lambda * \min(|K(u_N)|, 1)],$$

where  $C$  is a renormalizing constant so that step (iv) holds,

$$(2.2b) \quad C = \frac{\|\min(|K(u_N)|, 1)\|_\infty}{\|\mu_\lambda * \min(|K(u_N)|, 1)\|_\infty},$$

the cut-off function  $\chi_\delta$  is given by (1.12), and  $\mu_\lambda$  is the mollification kernel

$$(2.2c) \quad \mu_\lambda(x) = \frac{1}{\lambda} \exp\left(-\frac{10x^2}{(\lambda^2\pi^2 - x^2)_+}\right).$$

Two  $N$ -dependent parameters remain to be specified. Throughout, we will take the mollification width  $\lambda = 3\pi/N$ , and the lower cutoff  $\delta = \pi/N$ .

**2.1. Localized Viscosity (LV).** We define the localized viscosity (LV) scheme by

$$(2.3) \quad (u_N)_t + (P_N f(u_N))_x = \epsilon_N L(u_N) \cdot (u_N)_{xx}.$$

Hence this scheme amounts to the classical vanishing viscosity scheme (1.4) when  $L(u_N)(x) \equiv 1$ , i.e. at a discontinuity, and the inviscid scheme (1.3) when  $L(u_N)(x)$  vanishes.

**2.2. Localized Spectral Viscosity (LSV).** Instead of the full viscosity term in (2.3), we could add a spectral viscosity. The result is the localized spectral viscosity scheme (LSV)

$$(2.4) \quad (u_N)_t + (P_N f(u_N))_x = \epsilon_N L(u_N) [Q * (u_N)_{xx}].$$

This scheme switches between the spectral viscosity scheme (1.5) near discontinuities, and the inviscid scheme (1.3) elsewhere. It is therefore less dissipative than both the LV and SV schemes, and need not provide sufficient dissipation to control Gibbs' oscillations.

**2.3. Adaptive Spectral Viscosity (ASV).** Finally we consider a scheme that switches between full viscosity near discontinuities and spectral viscosity in smooth regions. This is the adaptive spectral viscosity scheme (ASV)

$$(2.5) \quad (u_N)_t + (P_N f(u_N))_x = \epsilon_N L(u_N) (u_N)_{xx} + \epsilon_N (1 - L(u_N)) [Q * (u_N)_{xx}].$$

Given the same choice of parameters, this scheme will be more dissipative than the SV, LV and LSV schemes. However, for the ASV scheme we use larger values of the cutoff frequency  $m$  than with the other schemes, with  $m = \frac{2}{3}N$  as a default choice.

More generally, one can let the choice of  $Q$  depend on  $u_N$  locally in space. This is only computationally efficient if a small number of coefficients  $Q$  is available, hence the ASV scheme (2.5) is a reasonable implementation of this idea, with the local dissipation given by either a standard SV choice of  $Q$  (1.6), the classical viscosity  $\hat{Q}_k = 1$  or a linear combination of the two. A related application of the localizer was put forth in [20], where polynomial reconstruction of pointwise data were taken to as high order as possible while only using data from a smooth region.

**2.4. Postprocessing.** Independent of which type of viscous regularization is employed, we expect to have a situation analogous to the one described in section 1.2: The approximation error  $u_N - u$  will be dominated by the  $\mathcal{O}(1/N)$  representation error  $P_N u - u$ . Therefore, after computing  $u_N(x, T)$  at a desired time  $t = T$ , we compute the postprocessed solution  $\tilde{u}_N(x, T)$  using (1.10) to recover spectral accuracy.

---

<sup>1</sup>Spectrally small amplitude of  $K(u_N)$  in smooth regions can be achieved by using exponential concentration factors, (page 1356) [3].

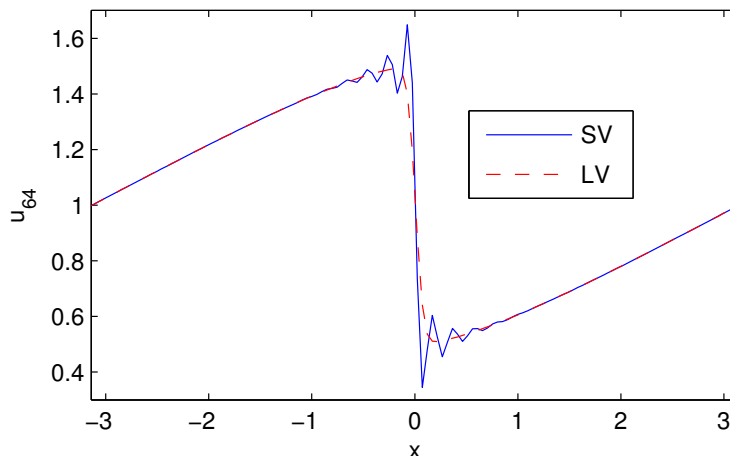


FIGURE 1. Solutions for Burgers' equation with smooth initial data

**2.5. Time discretization.** All the above schemes are semi-discrete in the sense that they take the form of ODE systems in time. We discretize time with the strong stability-preserving explicit fourth order Runge-Kutta method [5]. Hence, formally we can only expect fourth order accuracy. At low enough resolutions, however, it may be that errors related to the spectral spatial approximation dominates, hence one may still observe spectral accuracy in actual practice. The time step size is set to  $\Delta t = 1/2N$  in all our examples.

### 3. NUMERICAL STUDIES

We have presented four schemes that will be subject to numerical tests in this section. The schemes are SV (1.5) and LSV (2.4), both with cut-off frequency  $m = \sqrt{N}$ , ASV (2.5) with  $m = \frac{2}{3}N$  and LV (2.3). Our goals are to identify schemes that maintain spectral accuracy when shocks develop, and to compare the overall performance of the schemes relative to each other. For all the examples, we use the viscosity coefficient  $\epsilon_N = 4/N$ .

**3.1. Burgers' equation.** Consider Burgers' equation  $u_t + (\frac{1}{2}u^2)_x = 0$  subject to initial data

$$(3.1) \quad u_0(x) = 1 + \frac{1}{2} \sin(x).$$

The approximations  $u_N$  are sampled at  $t = \pi$  at which time a shock has formed and is located at  $x = 0$ . The solution profiles are shown in Figure 1. While SV yields visible oscillations near the shock, LV yields a smoothed profile reminiscent of a TVD (total variation diminishing) scheme. For a more detailed study of accuracy, we plot the errors of the postprocessed solutions in Figure 2. Spectral viscosity can be seen to yield the expected spectral convergence. In comparison, the localized viscosity scheme LV is significantly more accurate near the shock and at low resolutions. However, its convergence eventually stagnates. An explanation can be obtained from closely inspecting the solution profile: Although the LV scheme produces a near smooth shock profile, very small amplitude oscillations are still present in the smooth region, which could deteriorate performance at higher resolutions. Therefore, we turn to the ASV scheme as a compromise between local and spectral viscosity. Indeed, using ASV with cut-off at  $m = \frac{2}{3}N$  keeps the diffusive zone around the shock narrow as with LV, while removing the spurious oscillations. The result, as seen in Figure 2, is satisfactorily fast convergence comparable to SV, while we retain the improved efficiency of LV at low resolutions and near the shock. Finally, we test the LSV scheme. This scheme is clearly inferior to the others, in particular SV and ASV. Clearly too little dissipation is left in LSV after both spatial localization and spectral cut-off of viscosity.

For a more quantitative comparison of the ASV and SV schemes, we compute the average errors over all control points at least a distance 1 away from the shock, see Table 1. The observations based on the plots are confirmed. The more accurate behavior near the shock of the ASV scheme improves these error measures by

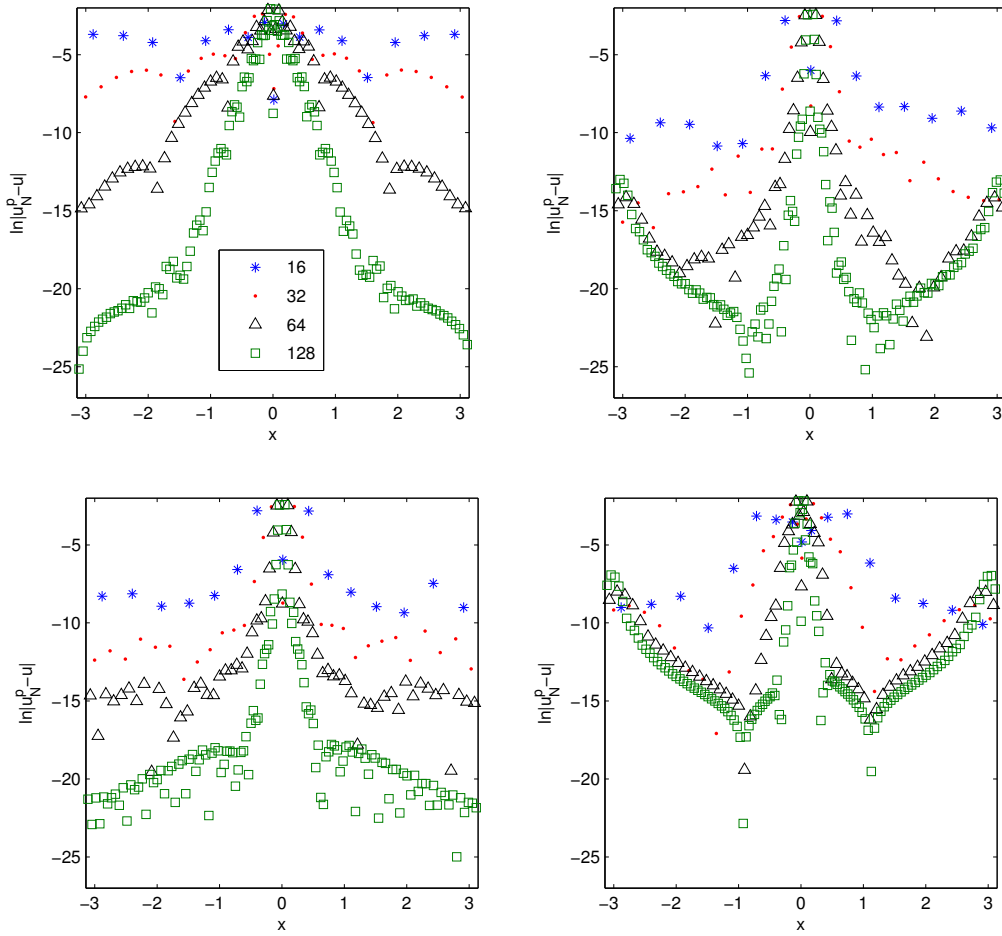


FIGURE 2. Burgers' equation with smooth initial data. Errors in postprocessed solutions  $\ln|\tilde{u}_N - u|$  at  $t = \pi$ . Top left: SV, top right: LV, bottom left: ASV, bottom right: LSV. The exact solution was calculated by characteristic tracing from the initial sample points.

	SV	ASV	ASV, $m = \sqrt{N}$	SV, $m = \frac{2}{3}N$
8	5.0e-2	1.6e-3	3.4e-3	4.7e-2
16	1.6e-2	2.3e-4	9.2e-4	1.4e-2
32	1.9e-3	9.4e-6	2.7e-4	7.4e-4
64	1.4e-5	4.3e-7	1.5e-5	3.4e-5
128	5.8e-8	3.6e-9	1.5e-8	7.6e-7
256	4.2e-10	9.2e-13	1.0e-12	9.4e-9

TABLE 1. Average error for checkpoints in  $|x| \in [1, \pi]$

orders of magnitude. We also provide error measures for alternative choices of cut-off frequencies  $m$ , which shows that they provide inferior results to their respective default values.

Computing solutions with rarefaction waves relies critically on sufficient dissipation to avoid unphysical shocks, hence it should be checked that new schemes can handle such a case. As an example, we consider initial data

$$(3.2) \quad u_0(x) = 1 - \frac{1}{2}\text{sign}(x).$$

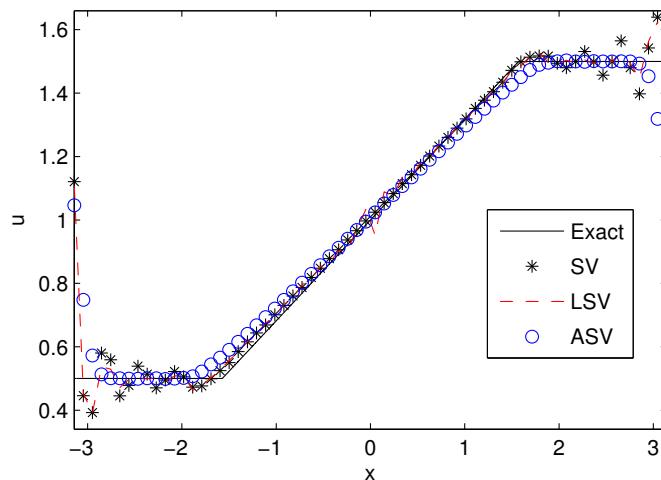


FIGURE 3. Burgers' equation rarefaction wave solution profiles.

Results are shown in Figure 3. We find that both SV and ASV provide satisfactory results, while LSV shows some signs of instability in the rarefaction fan. These initial data also produce a shock wave, for which the schemes perform much like in the first example.

**3.2. Buckley-Leverett equation.** Next, consider the nonconvex Buckley-Leverett equation

$$(3.3) \quad u_t + \left( \frac{v^2}{v^2 + (1-v)^2} \right)_x = 0, \quad v = \max(0, \min(1, u)).$$

This system is sensitive to what type of dissipative regularization is applied (e.g. [8]), i.e. different regularizations may converge to different weak solutions. First, we consider initial data  $u(x, 0) = \frac{1}{2} + \frac{1}{2} \sin(x)$ . Figure 4 shows results at time  $t = \pi$  after shocks were formed. The ASV and LV schemes produce stable, accurate results, much like in their performance in the convex case, while the SV scheme produces an apparently spurious solution. What appears to happen with SV is that the overshoots behind the shocks get interpreted as additional wave fronts. In order to look closer at this phenomenon, we repeat this experiment with a different form of the spectral viscosity filter  $Q$ , taking

$$(3.4) \quad \hat{Q}_k = \begin{cases} 0, & |k| \leq m \\ \exp(-(\frac{2m-k}{k-m})^2), & m < |k| < 2m \\ 1, & 2m \leq |k|. \end{cases}$$

This choice is based on [12], where a theoretical convergence rate of  $1/2$  was obtained. The results with (3.4) and cut-off  $m = \sqrt{N}$  are shown in Figure 5. The spurious wave is still present, but it appears to vanish slowly with resolution, a tendency that is not clear with our standard choice of  $Q$ . Errors from the LV scheme and the ASV scheme are in Figure 6. The ASV scheme yields fast convergence, while LV does not perform satisfactorily upon this close inspection.

Next, we consider Riemann initial data with  $u$  jumping from 0 to 1. The entropy solution consists of a compound wave that can be expressed analytically. The ASV scheme approximates the entropy solution quite well, see Figure 7, except for small artifacts behind the shock that appear to vanish with resolution. The SV scheme only slowly approaches the entropy solution even when the more dissipative viscosity filter (3.4) is used, see Figure 7.

**3.3. Shallow water equations.** This fluid equation system has a quadratic pressure-like term and a source term that models bottom topography. It takes the form

$$(3.5) \quad \rho_t + (\rho u)_x = 0, \quad (\rho u)_t + (\rho u^2 + \frac{1}{2} \rho^2)_x = -\rho z_x,$$

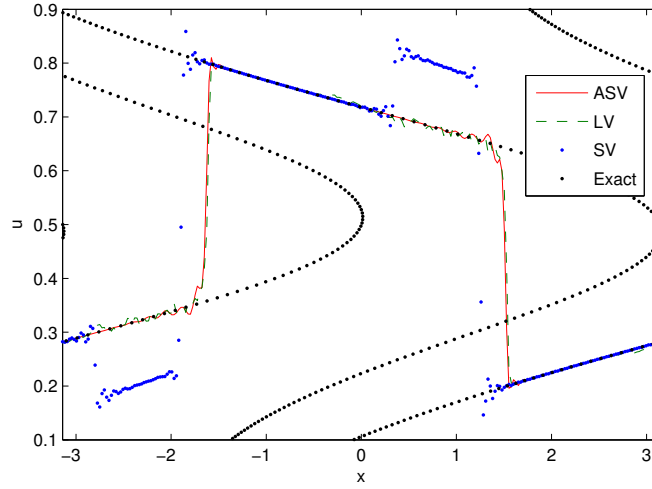


FIGURE 4. Solution profiles, initially smooth data for the Buckley-Leverett equation,  $N = 128$ ,  $t = \pi$ . ASV (solid), LV (stapled) and SV (dots). We compare to a multivalued solution based on tracing characteristics (stapled).

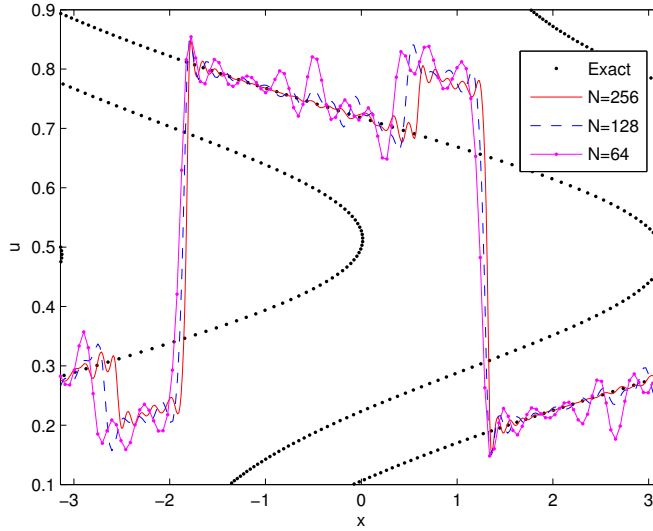


FIGURE 5. Solution profile, initially smooth data for the Buckley-Leverett equation. Refinement study of SV with  $Q$  given by (3.4).

where  $z$  is a given bottom topography that is fixed, i.e  $z_t = 0$ . As an example we consider

$$(3.6) \quad z(x) = \begin{cases} 0.1 \exp\left(\frac{x^2}{x^2 - 1.7^2}\right), & |x| < 1.7 \\ 0, & |x| \geq 1.7. \end{cases}$$

For initial data, the velocity  $u$  is set to zero, while  $\rho + z$  jumps from 0.2 to 0.4 at  $x = 0$ . For the shallow water system, we need to make some modification to the localizer: First, note that it is enough to consider the mass density profile  $\rho$  for detecting the shocks of this system, hence we use  $K(\rho_N)$ . Obviously the resulting localizer needs to be properly normalized. In order to normalize, we simply divide  $K(\rho_N)$  with the local value of  $\rho_N$  (before performing the modifications (2.2a)-(2.2c)).

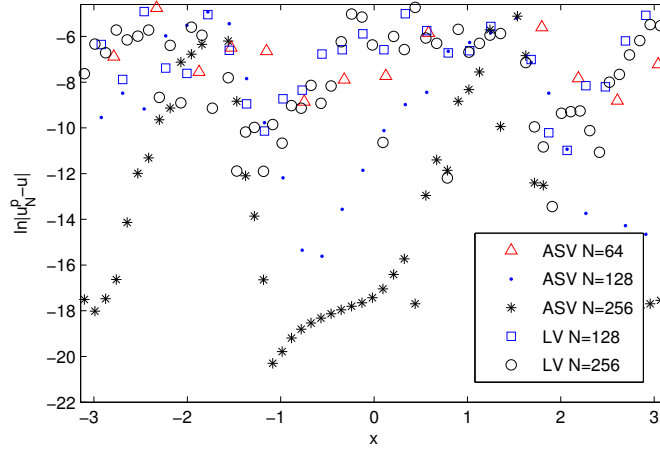


FIGURE 6. Errors, initially smooth data for the Buckley-Leverett. The postprocessing used  $\theta(x) = \min(|x - 1.62|, |x + 1.52|)/\pi$ .

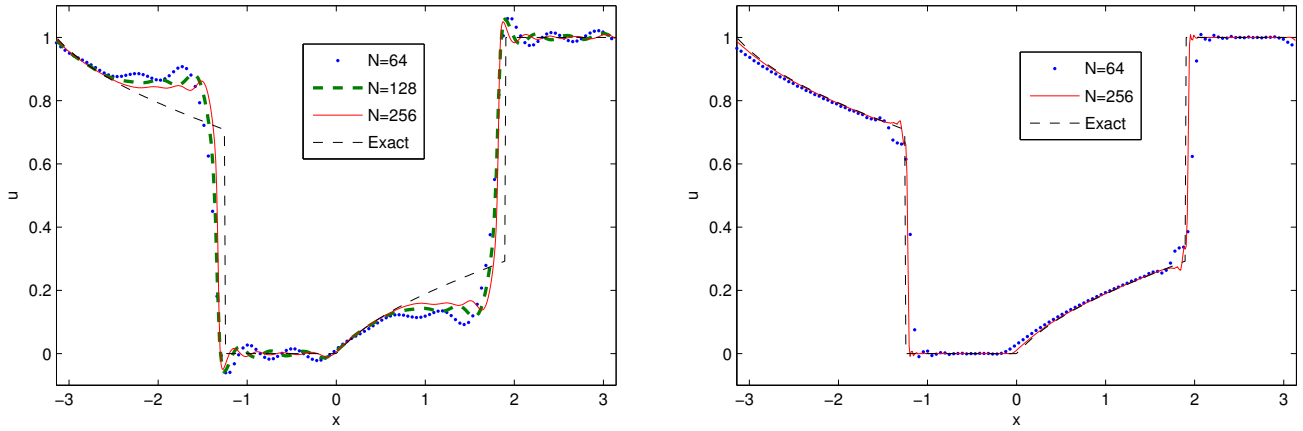


FIGURE 7. Riemann problem for Buckley Leverett equation at  $t = \pi/2$ . The SV method (left) vs. the ASV method (right)

The water height profiles  $\rho$  from ASV and SV at  $N = 256$  are plotted in Figure 8. ASV smoothes out the singularities somewhat, while SV shows a sharp profile with oscillations. As an error indicator, we show  $\ln|\tilde{u}_N|$ , the absolute value of postprocessed velocity, logarithmically scaled, in Figure 9. The postprocessing was performed assuming the singularities were at  $-2.5$ ,  $-0.6$ ,  $0.7$  and  $2.4$ . In the regions not yet affected by any waves, the exact solution is  $u = 0$ . We would want the schemes to retain at least 4th order accuracy in these regions. This expectation is confirmed sufficiently far from wave fronts, with ASV performing the best. The unprocessed velocity profiles at  $N = 256$  are shown in Figure 9. It is interesting to note that SV and ASV primarily differ near the singularities before postprocessing.

**3.4. Isothermal gas dynamics.** As another example system we look at

$$(3.7) \quad \rho_t + (\rho u)_x = 0, \quad (\rho u)_t + (\rho u^2 + p)_x = 0.$$

We consider Riemann initial data with  $u = 0$ , and  $\rho$  jumping from 1 to 0.5 at  $x = 0$ , yielding two Riemann problems due to periodicity. The resulting velocity profiles from SV and ASV are shown in Figure 10. In the regions not yet affected by any waves, the exact solution for the velocity is  $u = 0$ . Therefore, as an error measure, we plot  $\ln|\tilde{u}_N|$  in Figure 11. The ASV scheme shows the best accuracy, especially at low resolutions.

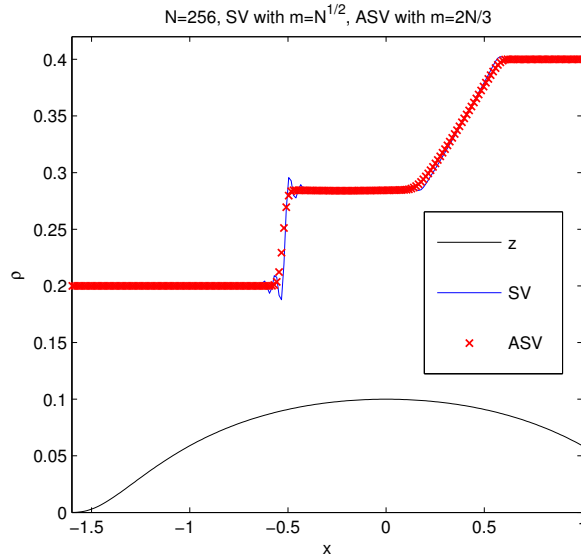


FIGURE 8. Shallow water problem. Water height for SV and ASV.  $z$  and  $\rho + z$  are plotted.

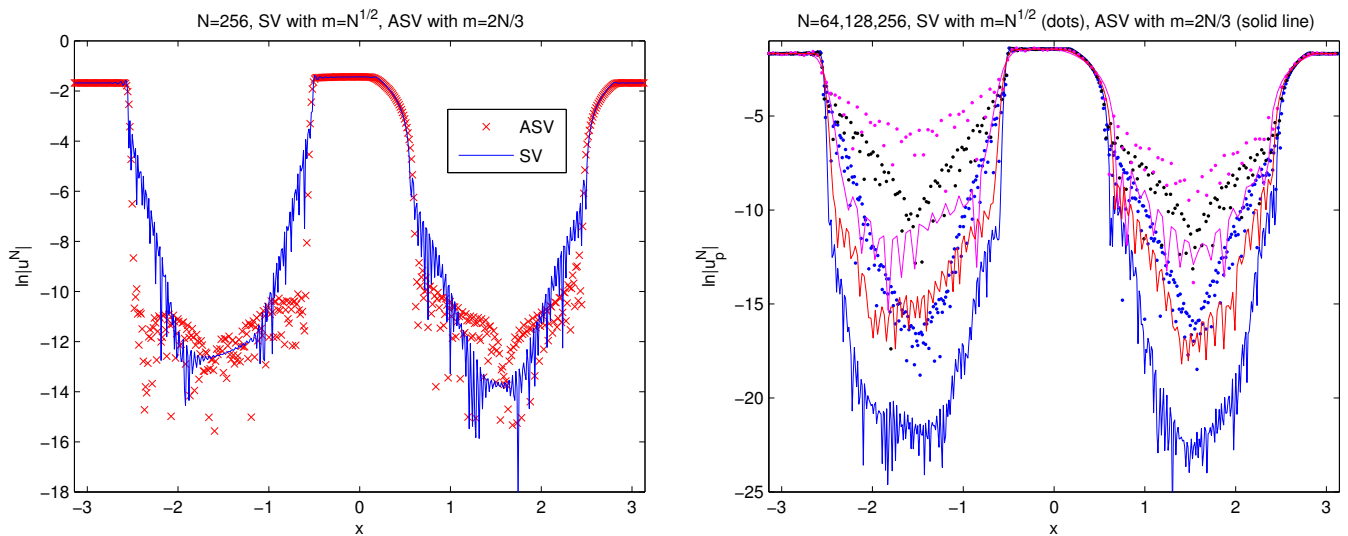


FIGURE 9. The shallow water problem. The velocity field for SV and ASV method pre-processed (left) vs. post-processed (right).

The postprocessing here is performed assuming the singularities are at  $1$ ,  $\pi - 1$ ,  $-0.9$  and  $-\pi + 0.9$ . We base the localizer on  $\rho$  in the same manner as described for the shallow water system above.

#### 4. CONCLUSION

We introduced the new adaptive spectral viscosity (ASV) scheme (2.5). The scheme combines the high accuracy of the spectral viscosity method with stabilizing diffusion applied only at discontinuities. The discontinuity locations are found with the spectral edge detection algorithm of [2, 3, 18].

The ASV scheme (2.5) was tested numerically and compared to the standard spectral viscosity method. We conclude that ASV offers significant improvement. In particular, for tests with Burgers' equation, isothermal gas dynamics and for shallow water with bottom topography, we obtained much better accuracy near the shock waves, and also significantly increased accuracy in the smooth regions. In particular, we observe a

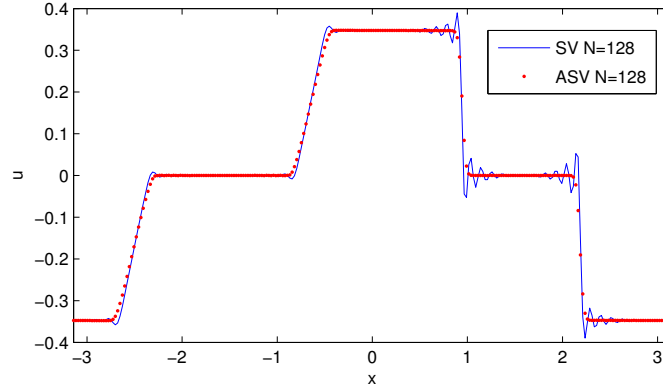


FIGURE 10. Velocity profiles for isothermal Euler Riemann problem. Solution sampled at  $t = \pi/4$ .

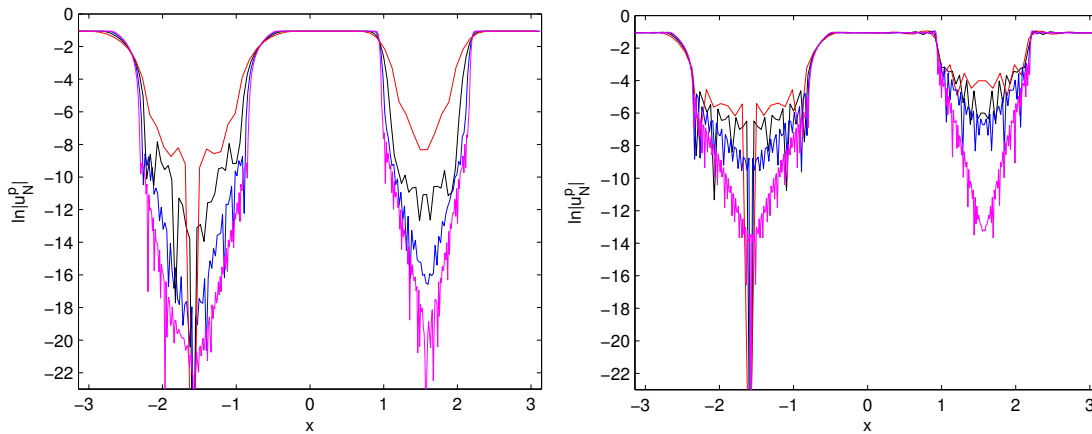


FIGURE 11.  $\ln|\tilde{u}_N|$  for isothermal Euler Riemann problem. ASV (left) and SV (right) solutions at  $N=32, 62, 128$  and  $256$ . Solution sampled at  $t = \pi/4$ .

strong improvement at low resolutions. In addition to ASV, we also tested the new local viscosity (2.3) and local spectral viscosity (2.4) schemes. They appeared stable, yet convergence was sometimes slow, indicating that they do not feature enough viscosity to control the Gibbs oscillations.

The Buckley-Leverett equation was used as a test case for treating scalar problems with non-convex fluxes. The entropy solution to this problem is unique, but it is known that the convergence of various approximate methods to *the* entropy solution in this case may depend on sensitive parameterizations; otherwise, the approximations may converge to other weak solutions. The standard spectral viscosity method had problems finding the entropy solution, although with sufficiently strong dissipation there appeared to be a slow convergence towards it. In contrast, the ASV method seems to be more robust, as it maintained high accuracy in the smooth regions also for the non-convex case.

The ASV scheme may be implemented efficiently using FFT techniques. It is straightforward to augment existing implementations with ASV since one only has to add new terms to an existing code, rather than changing it.

## REFERENCES

- [1] Majda A., J. McDonough, and S Osher. The Fourier method for nonsmooth initial data. *Math. Comp.*, pages 1041–1081, 1978.
- [2] Anne Gelb and Eitan Tadmor. Detection of edges in spectral data. *Applied and Computational Harmonic Analysis*, 7:101–135, 1999.

- [3] Anne Gelb and Eitan Tadmor. Detection of edges in spectral data ii. nonlinear enhancement. *SIAM J. Numer. Anal.*, 38(4):1389–1408, 2000.
- [4] Anne Gelb and Eitan Tadmor. Enhanced spectral viscosity approximations for conservation laws. *Appl. Numer. Math.*, 33(1-4):3–21, 2000.
- [5] C.-W. Gottlieb, S. Shu and E. Tadmor. High order time discretization methods with the strong stability property. *SIAM Review*, 43:89–112, 2001.
- [6] D. Gottlieb and E. Tadmor. Recovering pointwise values of discontinuous data within spectral accuracy. In *Progress and supercomputing in computational fluid dynamics; Proceedings of U.S.-Israel Workshop*, pages 357–375, 1985.
- [7] Ben-yu Guo, He-ping Ma, and Eitan Tadmor. Spectral vanishing viscosity method for nonlinear conservation laws. *SIAM J. Numer. Anal.*, 39(4):1254–1268, 2001.
- [8] Brian T. Hayes and Philippe G. LeFloch. Non-classical shocks and kinetic relations: Scalar conservation laws. *Archive for Rational Mechanics and Analysis*, 139:1–56, 1997. 10.1007/s002050050046.
- [9] Huiyuan Li, He-ping Ma, and Eitan Tadmor. Hyper spectral viscosity method for nonlinear conservation laws. *unpublished note*, 1999.
- [10] Yvon Maday, Sidi M. Ould Kaber, and Eitan Tadmor. Legendre pseudospectral viscosity method for nonlinear conservation laws. *SIAM J. Numer. Anal.*, 30(2):321–342, 1993.
- [11] Yvon Maday and Eitan Tadmor. Analysis of the spectral vanishing viscosity method for periodic conservation laws. *SIAM Journal on Numerical Analysis*, 26(4):pp. 854–870, 1989.
- [12] S. Schochet. The rate of convergence of spectral-viscosity methods for periodic scalar conservation laws. *SIAM J. Numer. Anal.*, 27:1142–1159, September 1990.
- [13] Chi-Wang Shu and Peter S. Wong. A note on the accuracy of spectral method applied to nonlinear conservation laws. *J. Sci. Comput.*, 10:357–369, September 1995.
- [14] E. Tadmor. Shock capturing by the spectral viscosity method. *Comput. Methods Appl. Mech. Eng.*, 80:197–208, July 1990.
- [15] E. Tadmor. Total variation and error estimates for spectral viscosity approximations. *Mathematics of Computation*, 60:245–256, January 1993.
- [16] Eitan Tadmor. Convergence of spectral methods for nonlinear conservation laws. *SIAM J. Numer. Anal.*, 26(1):30–44, 1989.
- [17] Eitan Tadmor. Super viscosity and spectral approximations of nonlinear conservation laws. In *Numerical Methods for Fluid Dynamics IV; Proceedings of the 1992 Conference on Numerical Methods for Fluid Dynamics*, pages 69–82. Clarendon Press, Oxford, 1993.
- [18] Eitan Tadmor. Filters, mollifiers and the computation of the gibbs phenomenon. *Acta Numerica*, 16(-1):305–378, 2007.
- [19] Eitan Tadmor and Jared Tanner. Adaptive mollifiers for high resolution recovery of piecewise smooth data from its spectral information. *Found. Comput. Math*, 2001.
- [20] Eitan Tadmor and Jared Tanner. An adaptive order godunov type central scheme. In *Hyperbolic Problems: Theory, Numerics and Applications; Proceedings of the 9th international conference in Pasadena, March 2002.*, pages 871–880, 2003.
- [21] Eitan Tadmor and Jared Tanner. Adaptive filters for piecewise smooth spectral data. *IMA Journal of Numerical Analysis*, 25(4):635–647, October 2005.

(Eitan Tadmor)

DEPARTMENT OF MATHEMATICS  
 CENTER OF SCIENTIFIC COMPUTATION AND MATHEMATICAL MODELING (CSCAMM)  
 INSTITUTE FOR PHYSICAL SCIENCES AND TECHNOLOGY (IPST)  
 UNIVERSITY OF MARYLAND  
 MD 20742-4015, USA  
*E-mail address:* `tadmor@cscamm.umd.edu`

(Knut Waagan)

CENTER OF SCIENTIFIC COMPUTATION AND MATHEMATICAL MODELING (CSCAMM)  
 UNIVERSITY OF MARYLAND  
 MD 20742-4015, USA  
*E-mail address:* `KWaagan@cscamm.umd.edu`